Technical Sciences
Academy of Romania
www.jesi.astr.ro

Journal of Engineering Sciences and Innovation
Volume 11, Issue 1 / 2026, pp. 31 - 44

A. Mechanical Engineering

Received ***22 October 2025*** *Accepted* ***11 March 2026***
Received in revised form ***22 January 2026***

Complex interfacial designs for mechanical performance in biodegradable bicomponent 3D printed parts

Maria Catana (Oancea)[1], Simona-Nicoleta Mazurchevici[1*], Harshit Dave[2], Virgil Teodor[3], Viorel Paunoiu[3], Dumitru Nedelcu[1,4]

[1]*„Gheorghe Asachi" Technical University of Iasi, Romania*
[2]*Sardar Vallabhbhai National Institute of Technology, Department of Mechanical Engineering, Surat 395007, India*
[3]*„Dunarea de Jos" University of Galati, Romania*
[4]*Technical Sciences Academy of Romania*

Abstract. Bicomponent and multimaterial fused filament fabrication (FFF) with biodegradable polymers offers a sustainable approach to producing structures with tailored mechanical properties. This study investigates the influence of interface geometry and printing parameters on the tensile performance of biodegradable FFF components. UltraFuse PLA Blue and PLA/PHA Shining Silver (Polylactic Acid/Polyhydroxyalkanoate) were used to print samples with four interface configurations: simple "T," double "2T," "dovetail," and "double dovetail," chosen to evaluate how interlocking complexity affects stress distribution, load transfer, and fracture behavior. Mechanical performance was assessed through uniaxial tensile testing, combined with fracture imaging and surface topography analysis. The results showed that both interface design and printing parameters, such as layer thickness and number of shells, significantly impact tensile strength. Thicker layers reduced filament-to-filament adhesion, particularly along the interface plane, while increasing the number of shells improved filament alignment along the loading direction but introduced potential transverse weaknesses. Among the configurations, the simple "T" interface exhibited the lowest cohesion and strength, whereas the "2T" and dovetail geometries promoted more uniform stress distribution and enhanced fracture resistance. These findings highlight the critical role of interface engineering in improving the mechanical reliability of biodegradable multimaterial FFF parts. Overall, the study demonstrates that simultaneous optimization of interface geometry and process parameters is an effective strategy for enhancing tensile performance, converting structurally vulnerable regions into mechanically robust zones, and providing practical guidance for the design of sustainable, high-performance biodegradable FFF structures.

∗Correspondence address: simona-nicoleta.mazurchevici@academic.tuiasi.ro

Keywords: biodegradable polymers, fused filament fabrication (FFF), interface geometry, multimaterial 3D printing, mechanical performance.

1. Introduction

Additive manufacturing via multimaterial fused filament fabrication (FFF) is increasingly recognized as a sustainable approach for producing components that combine biodegradability with tailored mechanical performance [1-4]. Unlike single-material printing, multimaterial FFF enables the creation of parts with locally optimized properties, integrating materials of varying stiffness, toughness, and functional behavior within a single component [5–9]. Such designs are particularly relevant in biomedical scaffolds, functional packaging, and lightweight structural components where material efficiency and environmental responsibility are essential. A central challenge in these systems is ensuring reliable adhesion between dissimilar polymers, as the interfacial zone dictates load transfer and determines overall mechanical integrity [10–12].

Polylactic acid (PLA) is the most commonly used biodegradable polymer for FFF due to its processability, dimensional stability, and favorable mechanical characteristics [13,14]. However, PLA exhibits limited ductility and is prone to brittle fracture, particularly under tension along the build direction [15–17]. To overcome these limitations, PLA can be combined with polyhydroxyalkanoates (PHA), a more ductile biopolymer, to create blends that retain biodegradability while improving toughness and energy absorption [18–20]. Nonetheless, differences in thermal and rheological properties between PLA and PHA can impair interfacial adhesion, creating weak zones that are susceptible to delamination under mechanical loading [21,22].

In addition to material selection, process parameters strongly influence mechanical performance. Extrusion temperature, layer thickness, print speed, raster orientation, and the number of shells determine filament wetting, interlayer diffusion, and the formation of voids [23–25]. For example, thicker layers increase deposition efficiency but reduce contact area, often diminishing filament-to-filament adhesion and initiating early cracks in critical regions [26–28]. Conversely, an increased number of shells improves tensile strength by aligning filaments along the load direction, yet it can introduce transverse weaknesses where shells meet infill, promoting local delamination [29–31]. Optimizing these parameters is therefore critical to achieving structural reliability while maintaining print efficiency.

Beyond processing conditions, interface geometry plays a pivotal role in improving mechanical performance. Strategies such as dovetail interlocks, stepped or gradient transitions, and hierarchical patterns inspired by natural structures (tendons, nacre, arthropod cuticles) have been shown to enhance adhesion area, redistribute stress, and delay crack propagation [32–40]. These approaches highlight the potential of geometry to transform traditionally weak regions into zones capable of bearing significant loads.

Despite these advances, the literature rarely examines the combined effects of interface geometry and process parameters in biodegradable multimaterial systems,

leaving a gap in comprehensive understanding of performance under realistic loading conditions [41–43]. Many studies address only material compatibility or process optimization in isolation, limiting predictive capability for real-world applications.

Globally, researchers are increasingly focused on the integration of material selection, interfacial geometry, and processing parameters to design multimaterial biodegradable components with predictable, high-performance characteristics,[44]. Within this context, the present study systematically investigates four engineered interface configurations (T, 2T, dovetail, double dovetail*) alongside variations in layer thickness and shell number. By correlating these variables with tensile behavior and fracture mechanisms, this research provides novel insights into the design of sustainable, mechanically robust FFF components, offering practical guidance for future applications in biodegradable multimaterial structures.

2. Materials and methods

Bicomponent samples were systematically designed to evaluate the influence of interface geometry on the mechanical behavior of fused filament fabrication (FFF) structures. Two biodegradable polymers were selected for this study: UltraFuse PLA Blue, [45] and PLA/PHA Shining Silver (Polylactic Acid/Polyhydroxyalkanoate), [46]. These materials were chosen due to their complementary mechanical characteristics and biodegradability, which make them suitable for multimaterial FFF applications. Four distinct interface configurations were considered: T, 2T mirrored about both axes of symmetry; dovetail; dovetail mirrored about both axes of symmetry. These geometries were selected to examine the effect of interlocking complexity on tensile strength, stress distribution, and fracture propagation.

The samples were fabricated using an Ultimaker 3 Extended 3D printer following the ISO 527 standard for tensile testing. The printing parameters were carefully controlled to ensure repeatability and minimize variability between samples. Specifically, the infill density was set to 100%, and all samples were oriented flat on the print bed. The build plate was maintained at 60 °C, while the extrusion temperature was 215 °C. The printing speed was kept at 60 mm/s, with a layer thickness of 0.3 mm and two/ four shells per sample. These settings were selected based on preliminary trials to optimize filament bonding and surface quality while preserving dimensional accuracy.

The specimens had dimensions according to ISO 527:2 standards. For each interface, three samples (A, B, C) were printed to highlight the stability of the process.

Mechanical characterization was carried out through uniaxial tensile testing using an Instron 3382 universal testing machine, following the ISO 527-3:2003 guidelines, room temperature.

In addition to mechanical testing, surface characterization was performed to assess printing quality and microstructural features at the interfaces. A Zygo profilometer

equipped with Mx Zygo software was employed to generate high-resolution topography maps of the sample surfaces. This analysis enabled the evaluation of surface roughness, filament fusion, and potential printing-induced defects, providing insight into correlations between surface morphology and tensile performance. By combining mechanical testing with surface topography analysis, the study aimed to elucidate the mechanisms underlying interface behavior in biodegradable multimaterial FFF samples.

3. Results and discussion

1. Tensile Tests

The tensile tests performed on the bi-material samples manufactured by FFF highlighted the decisive role of the interface design and the processing parameters on the mechanical behavior. For all four analyzed configurations (T, 2T, dovetail, and double dovetail), the failure mode and the achieved strength level were strongly correlated with the interconnection mechanism between the two materials and with the filament orientation relative to the loading direction.

The average experimental results of the uniaxial tensile tests on the bi-material samples printed from UltraFuse PLA–PLA/PHA for the four interface models are presented in Table 1.

Table 1. Average tensile properties of the 3D-printed samples

Crt.no.	**layer thickness**	**number of layers**	**interface**	**σ_{max} [MPa]**	**ε_t [%]**	**E [MPa]**
1	0.3	4	T	30.02±1.23	3.39±0.30	1149.93±52.09
2	0.3	2	2T	25.64±0.24	4.76±0.42	950.71±34.28
3	0.3	4	dovetail	15.23±0.60	1.62±0.17	1087.54±25.78
4	0.3	2	double dovetail	27.09±0.57	5.12±0.34	951.02±15.04

σ_{max} [MPa] - Tensile strength; ε_t [%] - Tensile strain at Break, E [MPa] - Modulus of Elasticity

Figure 1 shows the stress–strain behavior of samples with T, 2T, dovetail, and double dovetail interfaces, printed from UltraFuse PLA and PLA/PHA materials.

The *T-type interface* (Figure 9) exhibited the highest ultimate tensile strength, 30.02 ± 1.23 MPa (Table 1), which is associated with the presence of a larger number of shells (4) aligned favorably with the loading direction. However, fracture surface analysis revealed predominant separation along the material contact plane, indicating limited interfacial adhesion and a delamination-dominated failure mechanism (Figure 2). The increased stiffness provided by the four shells resulted in less ductile behavior and lower values of strain at failure.

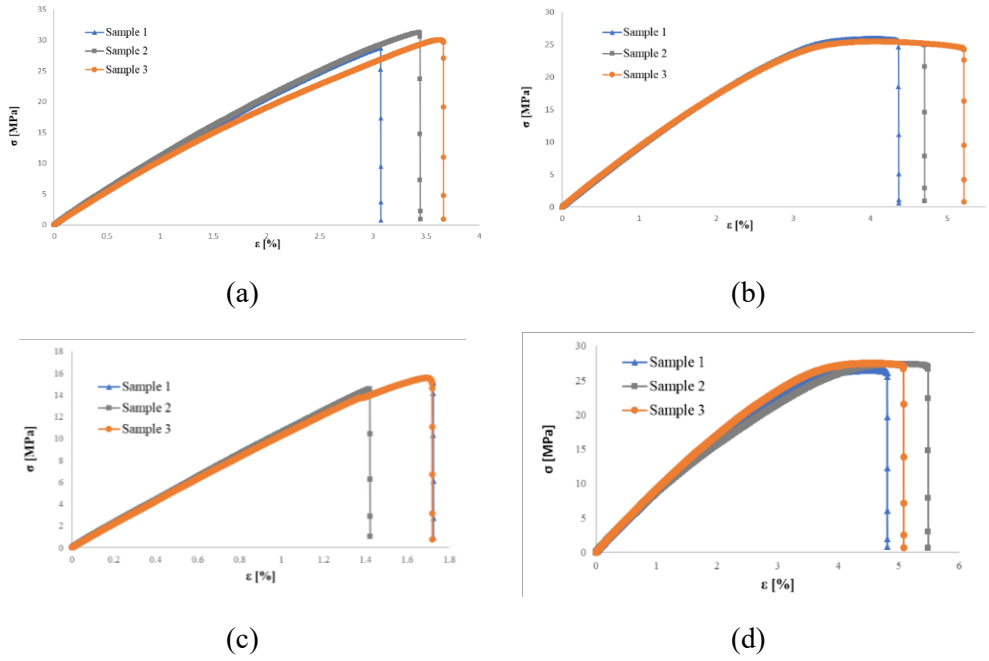

Fig. 1. Stress–strain behavior of bicomponent UltraFuse PLA–PLA/PHA 3D-printed samples: (a) T; (b) 2T; (c) dovetail; (d) double-dovetail

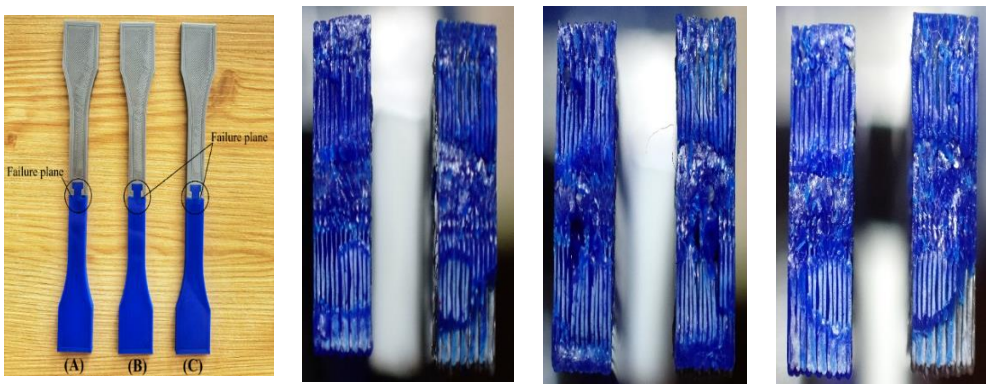

Fig. 2. Fracture regions of the T-interface samples: cross-sectional view of failure sample (A, B, C).

In contrast, the *2T configuration* (Figure 3) exhibited a more uniform stress distribution at the interface and a sufficiently high structural strength to prevent premature separation. In all samples, cracks propagated through the UltraFuse PLA material, away from the interface, indicating effective mechanical interlocking and optimal load transfer between the components. This behavior confirms that interface geometry can partially compensate for reduced interlayer adhesion caused by a layer thickness of 0.3 mm.

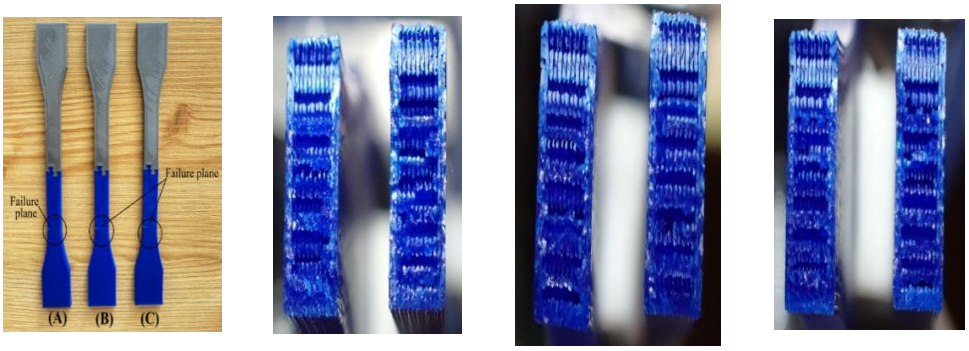

Fig. 3. Fracture regions of the 2T-interface samples: cross-sectional view of failure sample (A, B, C).

The *dovetail interface* samples (Figure 4) exhibited the lowest mechanical performance, with σ_{max} = 15.23 ± 0.60 MPa. Rapid failure, accompanied by a fracture zone localized near the interface, indicates the presence of stress concentrations in the narrowed regions of the design. In addition, the increased number of shells oriented transversely promoted crack initiation and accelerated propagation, resulting in minimal values of both strain at failure and tensile strength.

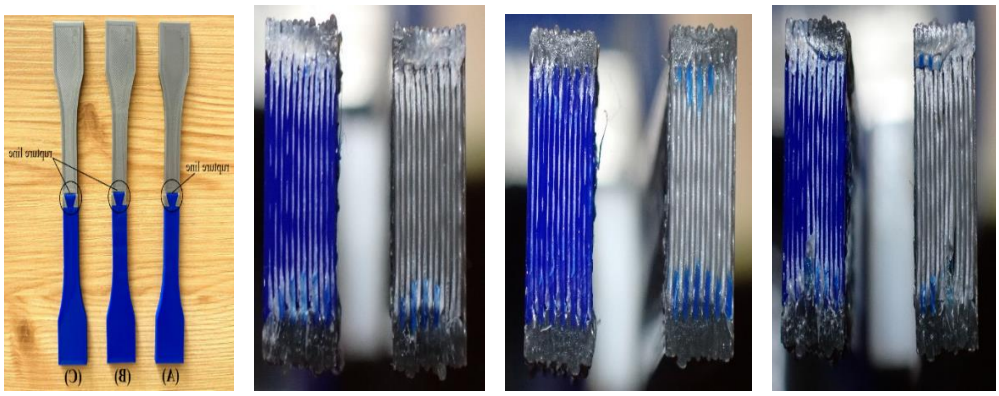

Fig. 4. Fracture regions of the dovetail -interface samples:
cross-sectional view of failure sample (A, B, C).

The best combination of strength and ductility was observed in the *double-dovetail configuration*. The increased contact area and interlocking geometry reduced the tendency for delamination, allowing for progressive energy dissipation during mechanical loading. Cracks propagated through the material rather than along the interface, which explains the high values of strain at failure and structural strength. Fracture occurred in all three samples (Figure 5) at similarly positioned regions within the UltraFuse PLA material, indicating consistent behavior among the samples. Regarding the tensile properties at failure, the values show homogeneity

(low dispersion), as illustrated in Figure 1(d). However, these experimental values are lower than those specified by the manufacturer, [45], due to the influence of the layer thickness (0.3 mm); a higher layer thickness negatively affects the tensile mechanical properties.

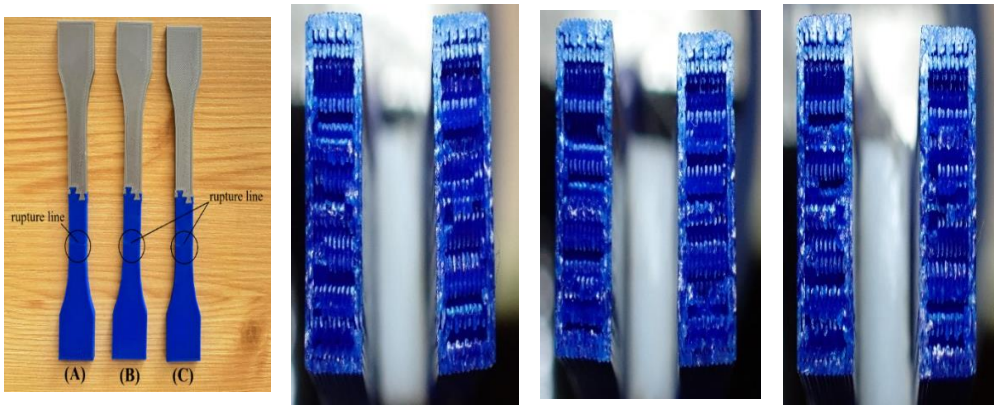

Fig. 5. Fracture regions of the double-dovetail -interface samples:
cross-sectional view of failure sample.

Zygo profilometry analyses reinforced these observations. The T and dovetail interfaces exhibited pronounced variations in surface topography, associated with insufficient interlayer bonding and potential defect initiation sites. In contrast, the 2T and double-dovetail samples displayed a more uniform profile and better filament continuity, which was subsequently reflected in improved mechanical durability.

2. Topographical characterization

The surface topography of the *T-type interface* exhibits pronounced relief variations, Figure 6, with depth differences on the order of tens of microns between contact regions. A clear alternation between elevated areas and steep depressions is observed, indicating non-uniform filament deposition across the interface plane.

The average width of the peaks is relatively large, suggesting partial fusion of the layers, but also the possible presence of voids at the edges. These irregularities are reflected in the profile plots, where abrupt amplitude variations indicate zones of discontinuous adhesion.

When correlated with the tensile test results, these features explain the occurrence of delamination and interfacial-plane failure, despite the maximum strength achieved. The limited interlayer adhesion, confirmed topographically by sharp peaks and irregular variations, resulted in increased stiffness but reduced ductility.

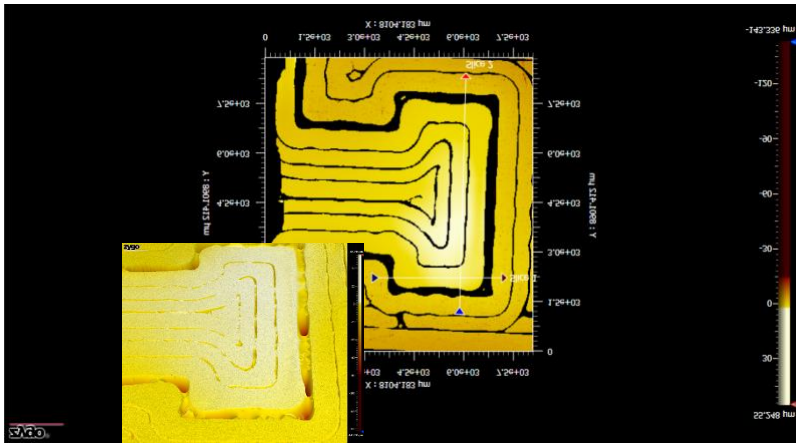

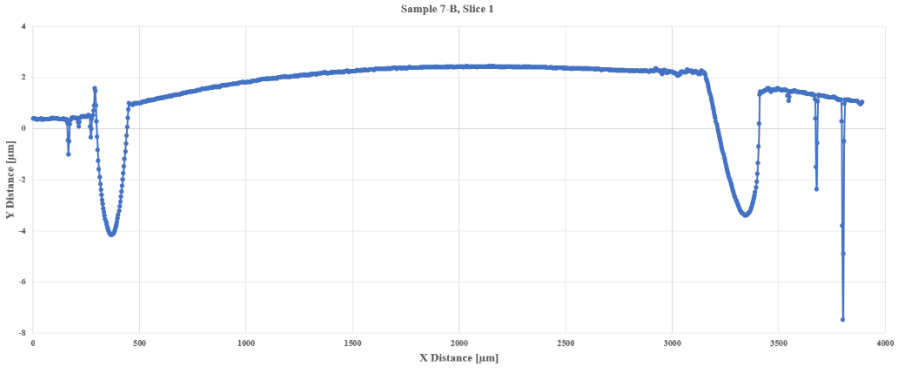

Variation of the slice 1 parameter for the T-interface sample

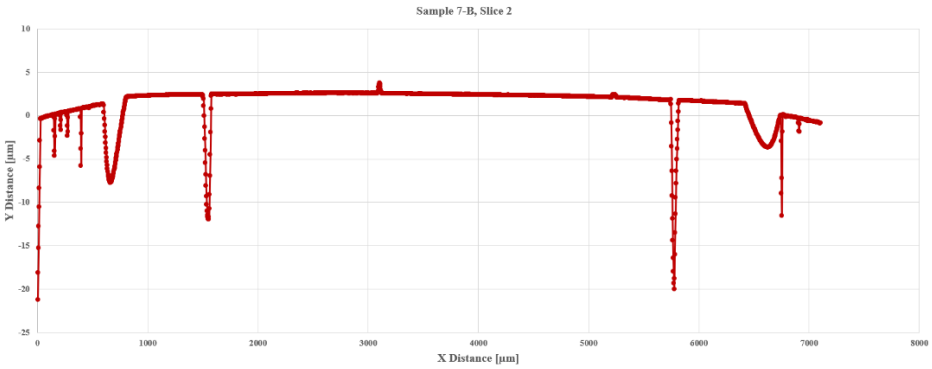

Variation of the slice 2 parameter for the T-interface sample

Fig. 6. Topographic analysis of the samples with T-type interface.

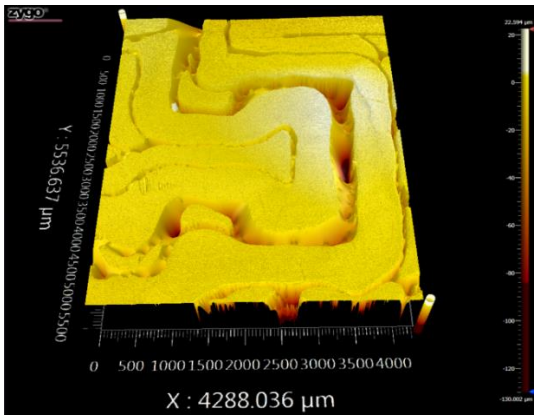

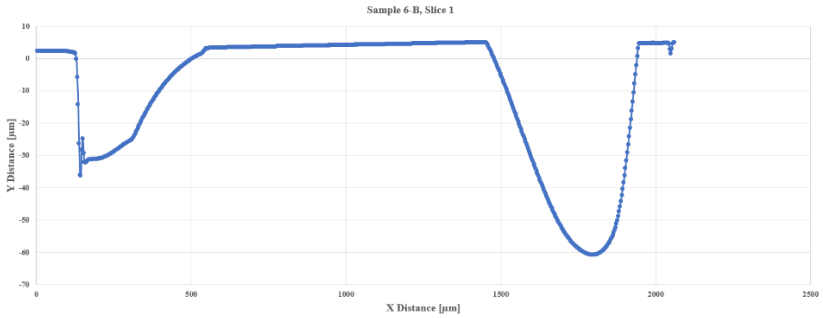

Variation of the slice 1 parameter for the 2T-interface sample

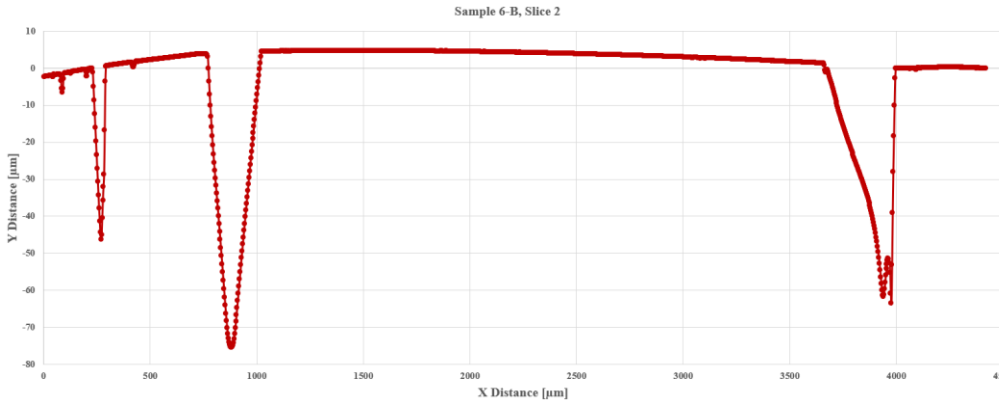

Variation of the slice 2 parameter for the 2T-interface sample

Fig. 7. Topographic analysis of the samples with 2T-type interface.

The surface topography of the *2T interface* exhibits a much more uniform profile, Figure 7, with moderate depths and a balanced distribution of peaks. Height variations are smoother, and peak widths are relatively consistent, indicating efficient interlayer fusion.

The profile plots show a clear reduction in maximum amplitude compared to the T interface, confirming better material continuity and uniform bonding across the surface.

When correlated with the mechanical results, this topographic behavior explains the high structural strength and crack propagation through the material rather than along the interface. The mechanical interlocking provided by the 2T geometry, combined with the uniform topography, allowed efficient load transfer between the components, preventing premature delamination.

The surface topography of the *dovetail interface* exhibits the largest relief variations, Figure 8, with pronounced depths and abrupt transitions between elevated and recessed regions. The peaks are sharp and narrow, indicating poor interlayer fusion and potential discontinuities in thermal contact during the FFF process. These differences are also reflected in the topographic plots, where steep slopes and sudden drops highlight potential defect initiation points.
When correlated with the tensile tests, these topographic inhomogeneities explain the rapid failure and the occurrence of cracks localized at the interface, particularly in the narrowed regions of the geometry. Stress concentrations in these areas promoted accelerated fracture propagation and reduced both tensile strength and strain at failure.

The surface topography of the *double-dovetail interface* exhibits the most balanced relief distribution, with wide peaks and shallow depressions, indicating uniform and efficient interlocking between the two materials, Figure 9.
The corresponding plots confirm a reduced variation in height parameters, suggesting complete filament fusion and excellent interlayer continuity. The consistent peak widths and absence of pronounced depressions indicate stable contact, without regions of separation.
These topographic features are fully consistent with the tensile test results: the double-dovetail interface demonstrated the best combination of strength and ductility, with cracks propagating through the material rather than along the interface. The extended contact area and uniform profile contributed significantly to reducing the tendency for delamination and enabling gradual energy dissipation during mechanical loading.

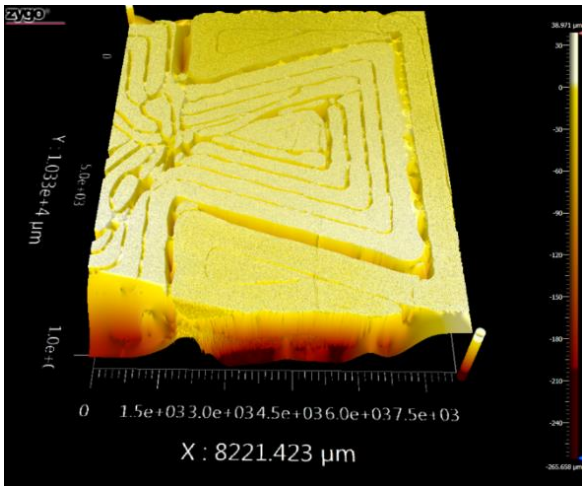

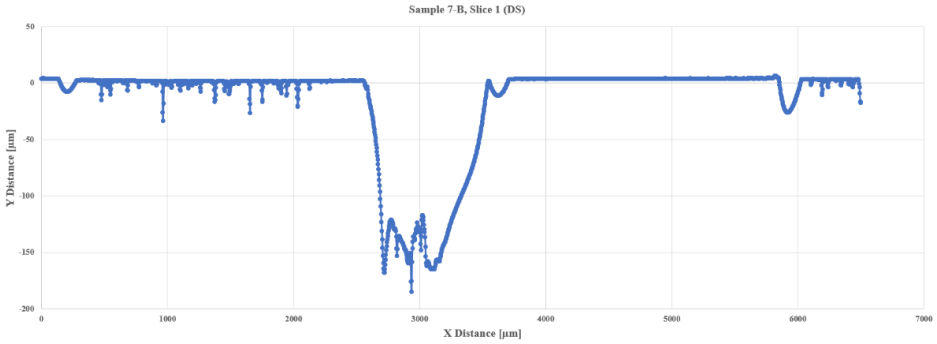

Variation of the slice 1 parameter for the dovetail -interface sample

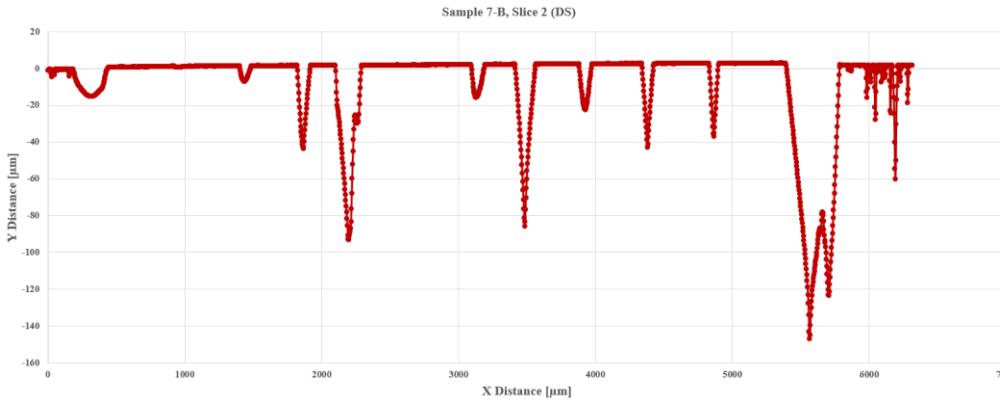

Variation of the slice 2 parameter for the dovetail -interface sample

Fig. 8. Topographic analysis of the samples with dovetail -type interface.

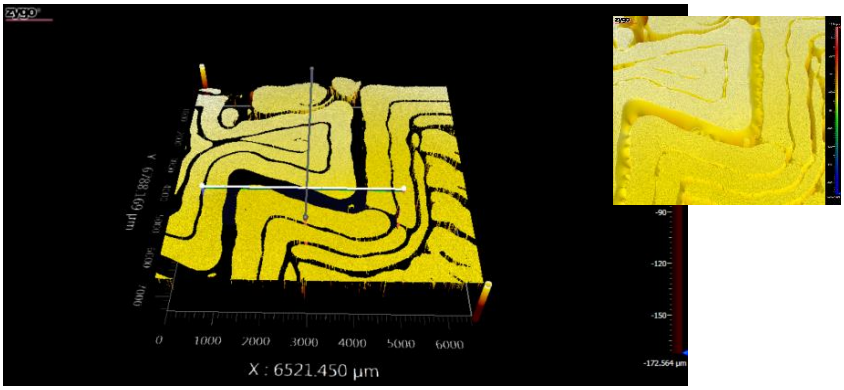

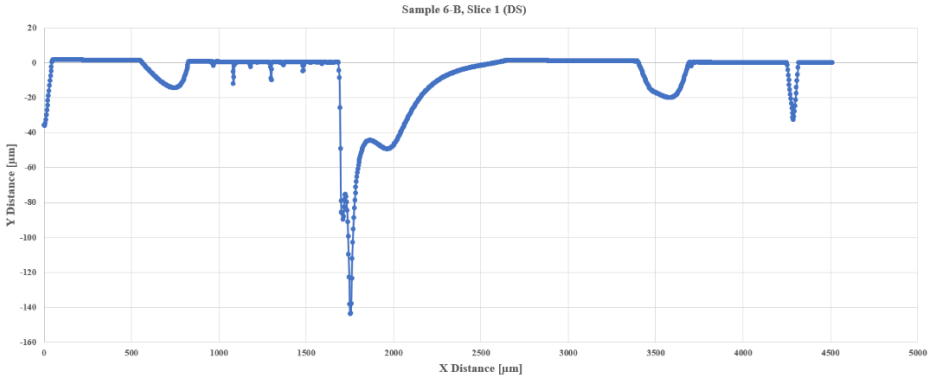

Variation of the slice 1 parameter for the double dovetail -interface sample

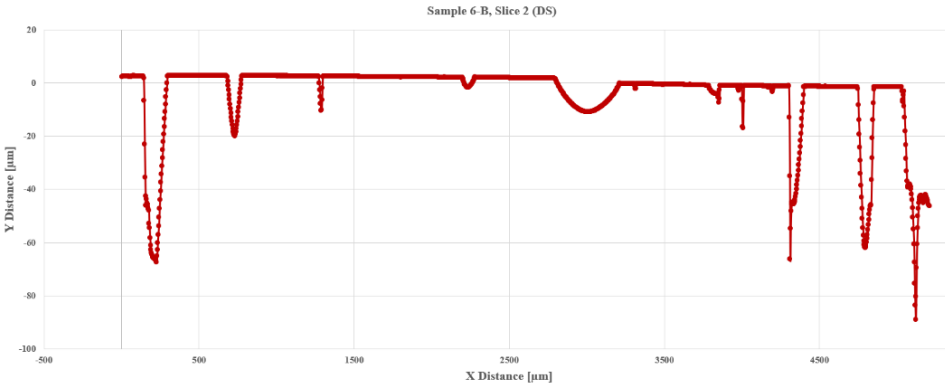

Variation of the slice 2 parameter for the double dovetail -interface sample

Fig. 9. Topographic analysis of the samples with dovetail -type interface

The combined analysis of topographic data and tensile test results indicates that interface surface uniformity is a direct indicator of adhesion and mechanical performance. Interfaces with large depth variations and narrow peaks (T and dovetail) exhibited delamination-driven fractures and lower mechanical values. In contrast, interfaces with uniform profiles and wide peaks (2T and double-dovetail) demonstrated efficient load transfer, effective mechanical interlocking, and superior ductile behavior.

4. Conclusions

The use of PLA-based biodegradable materials in bicomponent FFF systems represents a sustainable solution; however, the mechanical performance achieved depends significantly on interlayer bonding quality and the physico-mechanical compatibility between the components.

Processing parameters, particularly layer thickness and filament orientation, directly influence adhesion between materials. A larger layer thickness (0.3 mm) reduces thermal contact, thereby lowering tensile strength compared to the manufacturer's specifications.

Interface geometry plays a critical role in load transfer between the two materials. The 2T and double-dovetail interfaces provide effective mechanical interlocking and prevent delamination, in contrast to the T and dovetail configurations, which favor failure along the contact plane.

Tensile strength and failure mode are closely correlated with interface topography: surfaces with wide peaks and moderate relief variations promote uniform stress distribution, whereas abrupt topographies generate local stress concentrations and initiate premature cracks.

The combined topography–tensile analysis demonstrates that the simultaneous optimization of processing parameters and interface design can significantly improve the mechanical performance of biodegradable bicomponent structures, achieving an optimal balance between strength, ductility and sustainability.

References

[1] Wang Y.M. et al., *Multimaterial design strategies for AM*, Mater. Des., **220**, 2022, p. 110–124.
[2] Nazir A. et al., *Multi-material additive manufacturing review*, Mater. Des., **226**, 2023, 111661.
[3] Mazurchevici S.-N., Mazurchevici A.-D., Nedelcu D., *Dynamical Mechanical and Thermal Analyses of Biodegradable Raw Materials for Additive Manufacturing*, Materials, **13**, 8, 2020, 1819.
[4] Tzotzis A., Nedelcu D., Mazurchevici S.-N., Kyratsis P., *Surface Quality Evaluation of 3D-Printed Carbon-Fiber-Reinforced PETG Polymer During Turning: Experimental Analysis, ANN Modeling and Optimization*, Polymers, **16**, 20, 2024, p. 2927.
[5] Mazurchevici S.-N., Marguta A., Nedelcu D., *Characteristics of Biodegradable Polymers When Subjected to Ceramic Coatings*, Mechanics & Industry, **25**, 2024, p. 30.
[6] Nedelcu D., Mazurchevici S.-N., Popa R.-I., *Tribological and Structural Properties of Copper-Coated 3D-Printed Parts from Biodegradable Polymers*, Micromachines, 16, 1, 2025, p. 100.
[7] Lopes L.R. et al., *Functionally graded AM components*, Addit. Manuf., **47**, 2021, 102278.
[8] Hart K.R. et al., *Tailored regions in multimaterial AM,* Mater. Des., **189**, 2020, 108517.

[9] Vidakis N. et al., *Biopolymer use in structural AM parts*, Polymers, **13**, 2021, 1821.
[10] Wang X., Jiang M. et al., *Interlayer adhesion mechanics*, Rapid Prototyp. J., **22**, 2016, p. 109–123.
[11] Spoerk M. et al., *Amorphous–crystalline interfaces*, Addit. Manuf., **14**, 2017, p. 113–122.
[12] Coogan T.J., Kazmer D.O., *Polymer melt bonding*, Addit. Manuf., **24**, 2018, p. 90–102.
[13] Auras R. et al., *PLA characteristics review*, Macromol. Biosci., **4**, 2004, p. 835–864.
[14] Badia J.D. et al., *Recycled PLA performance*, Polym. Degrad. Stabil., **97**, 2012, p. 1881–1890.
[15] Chacon J.M. et al., *Orientation effects in PLA FFF*, Compos. Part B, **124**, 2017, p.143–152.
[16] Song Y. et al., *Fracture behavior of PLA*, Mater. Des., **123**, 2017, p. 221–230.
[17] Hsueh M.H. et al., *Weak interface in PLA*, Rapid Prototyp. J., **26**, 2020, p. 1501–1511.
[18] Castro-Aguirre E. et al., *PLA-PHA performance*, Prog. Polym. Sci., **54–55**, 2016, p. 51–68.
[19] Zhang K. et al., *PLA-PHA blends enhancement*, Mater. Sci. Eng. C, **76**, 2017, p. 318–325.
[20] Vegi K. et al., *PHA interface research*, Polymers, **14**, 2022, 546.
[21] Dwivedi R. et al., *Thermodynamic bonding in biopolymers*, Int. J. Adv. Manuf. Technol., **101**, 2019, p. 3225–3237.
[22] Tsai J. et al., *Interface fracture analysis*, ASME Open J. Eng., **1**, 2022, 011007.
[23] Li H. et al., *Process parameters–strength relationship*, Polym. Test., **86**, 2020, 106479.
[24] Luo C. et al., *Wetting and filament fusion*, J. Appl. Polym. Sci., **139**, 2022, 51726.
[25] Kantaros A., Piromalis D., *Layer effects*, Mater. Today Proc., **57**, 2022, p.927–934.
[26] Ning F. et al., *Void-strength correlation*, Compos. Part A, **142**, 2021, 106287.
[27] Correa D. et al., *Shell/infill delamination*, Addit. Manuf., **55**, 2022, 102844.
[28] Vijayakumar S. et al., *Shell-dominated mechanics*, Materials, **14**, 2021, 6547.
[29] Caminero M.A. et al., *Failure mechanisms*, Compos. Part B, **183**, 2020, 107688.
[30] Ribeiro M. et al., *Dovetail interlocks*, Mater. Des., **207**, 2021, 109854.
[31] Naghieh S. et al., *Interlocking patterns for AM joints*, Addit. Manuf., **36**, 2020, 101499.
[32] Parvez M.S. et al., *Stress-mitigating interfaces*, Mater. Des., **199**, 2021, 109402.
[33] Saldivar R.R. et al., *Bio-inspired interfacial toughening*, Addit. Manuf., **43**, 2021, 102010.
[34] Li X. et al., *Graded interlocks*, Compos. Sci. Technol., **208**, 2021, 108758.
[35] Mustafa K. et al., *Toughening via interlacing*, Polymers, **13**, 2021, 2142.
[36] Wu M. et al., *Geometric fracture constraints*, Compos. Struct., **285**, 2022, 115175.
[37] Chung H. et al., *Stress mapping multimaterial joints*, Mater. Des., **232**, 2023, 111960.
[38] Hasanov S. et al., *Multimaterial AM review*, Addit. Manuf., **52**, 2022, 102691.
[39] Wang H. et al., *Integrated structure–process effects*, Polymers, **15**, 2023, 1023.
[40] Rane K., Strano M., *A comprehensive review of multimaterial FFF mechanics and failure modes*, Compos. Part C, **10**, 2022, 100228.
[41] Vidakis N., Petousis M., Vairis A., *Interfacial performance in PLA biocomposites for AM*, Polymers, **13**, 2021, 2741.
[42] Spoerk M., Gonzalez-Gutierrez J., Cardon L., *Mechanical modeling of multimaterial interfaces in FFF*, Addit. Manuf., **47**, 2021, 102301.
[43] Rahman H., Letcher T., Venkatesan H., *Impact of interface geometry on strength in dual-material prints*, Mater. Today Commun., **33**, 2022, 104522.
[44] Camargo J.C., Machado C.Q., De Lima A.M., *Parameter–geometry correlation in PLA multimaterial tensile joints*, J. Manuf. Process., **68**, 2021, p. 810–822.
[45] https://www.filamente3d.ro/filamente/filament-ultrafuse-pla-blue-albastru-ral-5002-750g?srsltid=AfmBOoqLqZ6_ObY_N_d0WOAkbijR5xy8NbW6LfD2-l5it7sbMjS4aQZ4, accessed: October 2025.
[46] https://3dcompare.com/materials/product/colorfabb-shining-silver-plapha-2-85-mm/, accessed: October 2025.